JOURNAL OF Materials CHEMISTRY

Synthesis and characterization of copper containing mesoporous silicas

Michalis A. Karakassides,*[a] Athanassios Bourlinos,[a] Dimitris Petridis,[a] Liliane Coche-Guerènte[b] and Pierre Labbè[b]

[a]*National Center for Scientific Research "Demokritos", Institute of Materials Science, 15310 Ag. Paraskevi, Attikis, Athens, Greece*
[b]*Laboratoire d'Electrochimie Organique et de Photochimie Redox (URA CNRS 1210), Universite Joseph Fourier Grenoble 1, BP 53, 38041 Grenoble Cedex 9, France*

Received 8th June 1999, Accepted 7th December 1999

A series of copper containing mesoporous silicas has been prepared at room temperature using tetramethylorthosilicate as the source of silicon, a quaternary ammonium chloride salt as organic template surfactant and copper complexes obtained from organofunctional silicon molecules as ligands. Using this synthetic route, it was possible to prepare mesoporous materials containing up to 4.7 wt% copper. The structure and the sorption properties of the obtained materials have been studied by X-ray diffraction, Fourier-transform reflectance IR spectroscopy, transmission electron microscopy and surface area measurements. All experimental data reveal that calcined products containing up to 2.4 wt% copper retain the basic structural characteristics of MCM-41 materials, while higher copper loading leads to progressive destruction of hexagonal structure. Electron paramagnetic resonance was used to study the symmetry and environment of Cu(II) species in the silicate framework of the as synthesized and calcined materials, as well as the accessibility of these centers to polar adsorbed molecules, such as pyridine. The spectra of calcined materials indicate a distorted octahedral geometry for the Cu(II) centers which were easily accessible by pyridine molecules. Cyclic voltammetry showed that calcined copper containing mesoporous samples exhibit a marked electroactivity indicating that most of the copper centers are distributed on the mesoporous surfaces.

Introduction

An important class of inorganic materials with large internal surface area and high pore volume, designated as MCM-41, has recently emerged.[1,2] As these materials display cylindrical pores with diameters in the range 20–100 Å, they show potential promise as effective absorbents and catalysts in processes involving large molecules that can diffuse freely through their pores. However, since mesoporous pure silica does not show exchange properties, incorporation of metal centers in the silicate framework is necessary for their use in catalysis. Several attempts have been made to prepare MCM-41 based materials with various amounts of Al or other metals,[3–6] which can endow silica with desirable properties. Thus, the substitution of framework silicon by other tetravalent or trivalent metal ion such as Ti^{4+}, Sn^{4+}, B^{3+}, Al^{3+},Cr^{3+} *etc.*, has led to modified MCM-41 structures containing variable amounts of these ions.[7–11] On the other hand, the presence of divalent metals in the silica framework is also desirable for catalytic and other applications. For the synthesis of M(II)-substituted silica the following three methods have been described: (i) ion exchange of mesoporous matrix with a metal salt solution,[12,13] (ii) grafting the inner walls of mesoporous silica with an organometallic complex[14,15] and (iii) incorporation of metal oxide centers into the mesoporous structures by direct insertion of metal ions as precursors in the initial stage of synthesis.[16,17] Recently, a new sol–gel method for the incorporation of divalent metal ions into mesoporous silica was reported.[18] The method relies on the use of organofunctional silicon alkoxides of the type $(RO)_3Si–X–A$ (A represents an organic functional group and X is a hydrolytically stable spacer), which have the ability to form metal complexes that are similar to those formed from the corresponding ligands without the $(RO)_3Si$ group. These organically substituted alkoxides, after binding to metal ions (*e.g.* Cu^{2+}), can undergo co-condensation with $Si(OR)_4$ units by the sol–gel route to yield metal implanted mesoporous silicas.[19,20] The main advantages of the sol–gel method are the possibility to incorporate higher concentrations of metal centers in the silica framework and the resulting homogeneous distribution in the resulting porous structure.

In this work, we explore in detail the ability of $(RO)_3Si–X–A$ derivatives to bind M(II) centers and report the synthesis and characterization of MCM-41 materials modified with Cu^{2+} ions. The structure and sorption properties of the obtained materials were studied by X-ray diffraction (XRD), transmission electron microscopy (TEM), IR reflectance spectroscopy (FTIR) and surface area measurements. The environment and accessibility of the incorporated Cu^{2+} centers were studied using electron paramagnetic resonance (EPR) and cyclic voltammetry (CV).

Experimental

Synthesis of copper containing MCM-41

Cu-containing MCM-41 materials were synthesized by a sol–gel approach using $Si(OCH_3)_4$ as the silicon source and complexes of the type $\{[(CH_3O)_3Si(CH_2)_3NHCH_2CH_2NH_2]_2\}Cu$, formed from copper and commercially available *N*-[3-(trimethoxysilyl)propyl]ethylenediamine (DIAMO) in a molar ratio of 1 : 2. This ratio proved to be the optimal in order to obtain well ordered solids. The precursor metal complexes were prepared *in situ* and then mixed with $Si(OCH_3)_4$ in the presence of a water–methanol solution of hexadecyltrimethylammonium chloride to yield mesoporous silicas containing $Cu[NHCH_2CH_2NH_2(CH_2)_3SiO_3]_2$ centers. During the preparation the $(CH_3O)_3Si–$ segments of the Cu complex were easily hydrolyzed and participated in network condensation. The solid products were then calcined at 600 °C in air to remove

Table 1 Chemical composition and structural properties of calcined MCM materials

Sample	Cu(wt%)	d_{100}/nm	a_o/nm	Wall thickness/nm	BET surface area/m^2 g^{-1}
MCM-41	0	3.0	3.5	1.7	1021
Cu40-MCM	1.2	3.2	3.7	2.0	1116
Cu20-MCM	2.4	3.3	3.8	2.0	988
Cu10-MCM	3.4	3.0[a]	3.5	—	—
Cu05-MCM	4.7	3.6	4.2	2.5	580

[a]This sample exhibits a maximum at 3.0 nm and an intense shoulder at 3.2 nm. This is indicative of the presence of two different pore size distributions.

all organic components. The heat treatment, however, did not remove the Cu(II) centers as indicated by the pale blue colour of the synthesized samples. The results of chemical analysis for calcined samples from different DIAMO/TMOS ratios are given in Table 1.

In a typical preparation, 1 mmol of DIAMO was added dropwise to a methanolic solution of copper(II) chloride (0.5 mmol in 5 ml methanol). The resulting dark blue solution was then added under stirring to 20 mmol $Si(OCH_3)_4$ and the mixture was left for 3–4 min. The clear solution was added to a stirred solution containing 34 ml of distilled water, 7 ml of methanol, and 2.76 mmol of hexadecyltrimethylammonium chloride. After a few seconds a dark blue solid was precipitated. The product, designated as MCM-Cu(2.4) (the number in parentheses indicates the wt% copper in the calcined sample) was allowed to age for 3 h, and then filtered off, washed extensively with distilled water and methanol, dried in air and finally calcined at 600 °C for 5 h (heating rate 0.2 °C min^{-1}). The material was pale blue indicating the incorporation of copper ions into the mesoporous framework. Mesoporous materials with various amounts of copper were prepared by varying the DIAMO/TMOS ratio, from 40 to 5, but always keeping the total Si to surfactant ratio at a fixed value of 7.6.

For EPR spectral comparisons, a MCM-41 sample containing *ca.* 4.7 wt% copper was prepared by impregnation of the appropriate amount of copper chloride salt in methanol. The as recovered wet impregnated sample was dried at 150 °C for 2 h prior to EPR measurements.

Physical measurements

X-Ray powder diffraction data were collected on a D500 Siemens diffractometer using Cu-Kα (40 kV, 35 mA) radiation and a secondary beam graphite monochromator. Diffractograms were collected in the 2θ range 1–10°, in steps of 0.01° and a counting time of 1 s per step. IR reflectance spectra were measured with a Nicolet 550 infrared spectrometer equipped with a DTGS detector. Absorption coefficients were calculated after a Kramers–Kröning inversion of the reflectivity spectra and using the equation $a = 4\pi v\varepsilon''/n$ where ε'' is the imaginary part of the dielectric constant (relative permittivity), n the refractive index and v the frequency (cm^{-1}). Chemical analysis was performed with a Perkin-Elmer 3000 ICP spectrometer. The N_2 adsorption–desorption isotherms were measured at −196 °C on a Quantachrome Autosorb-I porosimeter. BET surface areas were calculated from the linear part of the BET plot according to IUPAC recommendations. The pore size distribution was estimated from the absorption isotherm using a cylindrical pore model.[21] Transmission electron micrographs were taken on a 200 kV Philips CM20 microscope. Electron paramagnetic resonance (EPR) spectra were obtained using a Bruker ER 200D-SRC spectrometer equipped with an Oxford ESR 9 cryostat, a Bruker 035M NMR-gaussmeter and an Anritsu MF76A microwave frequency counter. Spectra were recorded at 10 K and collected on a PC interfaced to the spectrometer.

Electrochemical studies were performed with a conventional three-electrode potentiostatic system. A PAR model 173 potentiostat with a model 175 programmer and a Sefram TGM 164 XY/t recorder were used. In order to study the electroactivity of the insulating mesoporous powders, we mixed them (10 mg) with graphite powder (10 mg). The resulting mixtures were then pressed on a Teflon coated carbon tissue (10 mm diameter disk) using IR pellet equipment (the applied force was 3.5 tonne cm^{-2} for 5 min). The resulting pellets exhibited excellent mechanical properties and could be picked up with a gold wire in order to perform electrical connection with an external circuit, or supported by a gold grid inserted in a specially designed Teflon frame. All potentials were referred to an Ag|Ag^+ (10 mM) reference electrode. The potentials were cycled with a sweep rate of 10 mV s^{-1}. The electrolyte, 0.1 M NEt_4ClO_4 in dry acetonitrile, was extensively deoxygenated by purging with N_2.

Results and discussion

Structural characterization and sorption properties of as-synthesized and calcined copper containing MCM-41 samples

Fig. 1 shows the powder XRD patterns from as synthesized and calcined copper containing MCM-41 samples prepared from different molar ratios of TMOS/DIAMO. The patterns show a characteristic strong diffraction at low scattering angle 2θ, corresponding to d_{100} spacings in the range 41–32 Å for the as synthesized samples. Calcined samples show a decrease in the

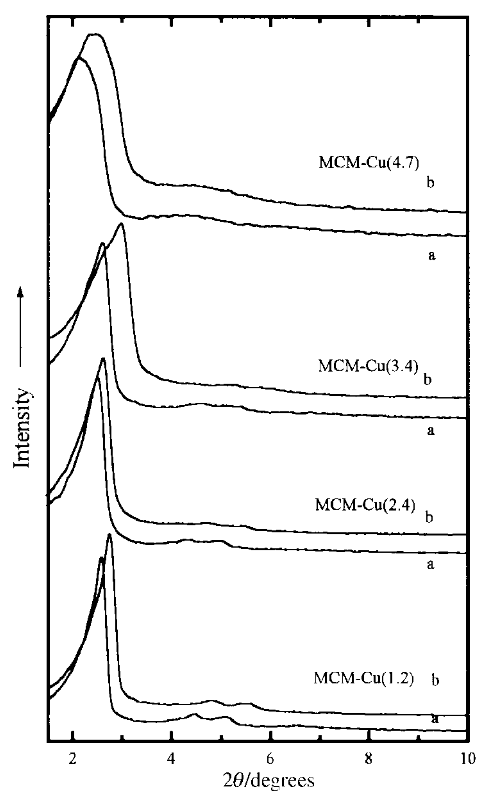

Fig. 1 Powder X-ray diffraction patterns of MCM-41 samples containing different amounts of copper: (a) as synthesized and (b) after calcination at 600 °C.

d_{100} spacing compared to the as synthesized samples. The decrease in d_{100} reflects a shrinkage in the pore diameters upon calcination. Calcined MCM-Cu(1.2) and MCM-Cu(2.4) exhibit sharper d_{100} reflections accompanied by better resolved 110 and 200 reflections than those of MCM-Cu(3.4) and MCM-Cu(4.7) materials. The higher order Bragg reflections, indicative of hexagonal phases, lose intensity after calcination but are still well resolved in the patterns of MCM-Cu(1.2) and MCM-Cu(2.4) (Fig. 1). These reflections become weak and diffuse as the concentration of copper increases, *i.e.* in MCM-Cu(3.4) and MCM-Cu(4.7), implying poor crystallinity. Attempts to prepare modified MCM-41 with greater amounts of copper (>5 wt%) gave XRD patterns without the characteristic d_{100} reflection suggesting loss of long range packing order. Combining the XRD and chemical analysis data (Table 1) we conclude that the best results, *i.e.* maximum copper loading and long range hexagonal order, are achieved with *ca.* 2.5 wt% copper.

The N_2 adsorption–desorption isotherms for the MCM-Cu(2.4) sample and the corresponding pore size distribution curve calculated using a cylindrical pore model[21] are shown in Fig. 2. The shape of the isotherms is typical of a MCM-41 material prepared by hydrothermal synthesis.[22] A well defined step in the adsorption curve, near $P/P_o = 0.2$ indicates filling of the framework-confined mesopores. The sample exhibits a high surface area of *ca.* 1000 $m^2\ g^{-1}$, while from the pore size distribution curve the pore diameter is calculated to be *ca.* 20 Å. Combining these data with the XRD data of the same sample, we can determine the framework wall thickness by subtracting the mesopore size from the repeat distance a_o between pore centers given by $a_o = 2d_{100}/\sqrt{3}$ from which the wall thickness is found to be 20 Å. This value is somewhat larger than the wall thickness of a MCM-41 sample prepared from $Si(OCH_3)_4$ without copper (17 Å). This increase can be ascribed to the participation of some of the Cu–DIAMO complex in building the framework walls of the as synthesized sample. A large framework wall thickness is desirable for improved thermal stability.

Fig. 3(a) shows the transmission electron microscopy (TEM) lattice image of calcined MCM-Cu(1.2). The material exhibits a long range hexagonal ordering of the channels. The size of mesopores estimated by TEM is in good agreement with the value determined from adsorption and XRD experiments. From the representative hexagonal ordering of the channels [Fig. 3(b)] the following unit cell parameters can be obtained, $a_o = 40$ Å, pore diameter = 20 Å, wall thickness = 20 Å, values which compare well with $a_o = 37$ Å, pore diameter = 17 Å and wall thickness = 20 Å, calculated from adsorption and XRD results.

IR spectra of the as synthesized and calcined MCM-Cu(2.4) samples are shown in Fig. 4. Spectrum (a) from an as synthesized sample shows bands at 1047, 954, 792 and 445 cm^{-1}. Bands at similar wavenumbers in the spectra of crystalline and amorphous SiO_2 have been assigned to characteristic vibrations of Si–O–Si bridges crosslinking the silicate network.[23–26] Thus, the stronger band at 1047 cm^{-1} in Fig. 4(a) can be assigned to the asymmetric stretching mode vibration of the Si–O–Si group whereas the bending motion of oxygens in the same bridge is responsible for the band at 792 cm^{-1} (motion along the bisector of the Si–O–Si bridging group). In addition, the rocking motion of bridging oxygens perpendicular to the Si–O–Si plane can be correlated with the 445 cm^{-1} band. All these Si–O bands show increases in wavenumber upon heat treatment at 600 °C, indicating a further condensation of Si–O–Si bridges that increases the crosslinking of the silicate framework [Fig. 4(b)]. Finally, the band at 954 cm^{-1}, which originates from the presence of $Si-O^-$ and Si–OH bonds in silicate tetrahedral units, decreases in intensity upon heat treatment. This is an expected result since calcination of the as synthesized MCM material leads to dehydroxylation of the silicate surface and removal of the

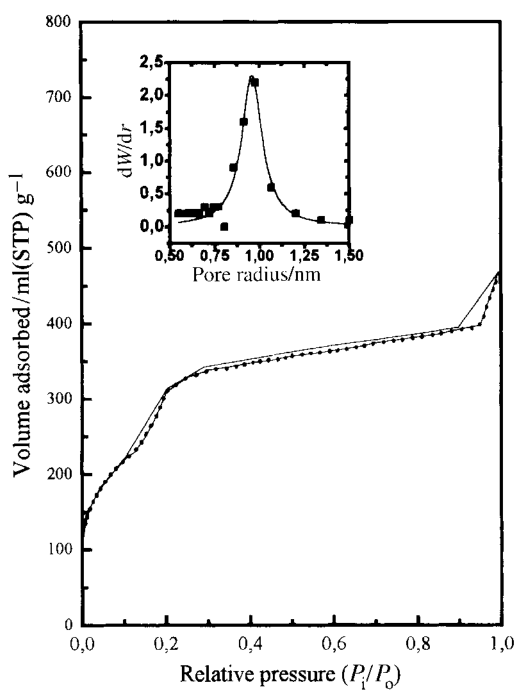

Fig. 2 Nitrogen adsorption–desorption isotherms for calcined MCM-Cu(2.4). Inset, pore distribution calculated from the N_2-adsorption branch.

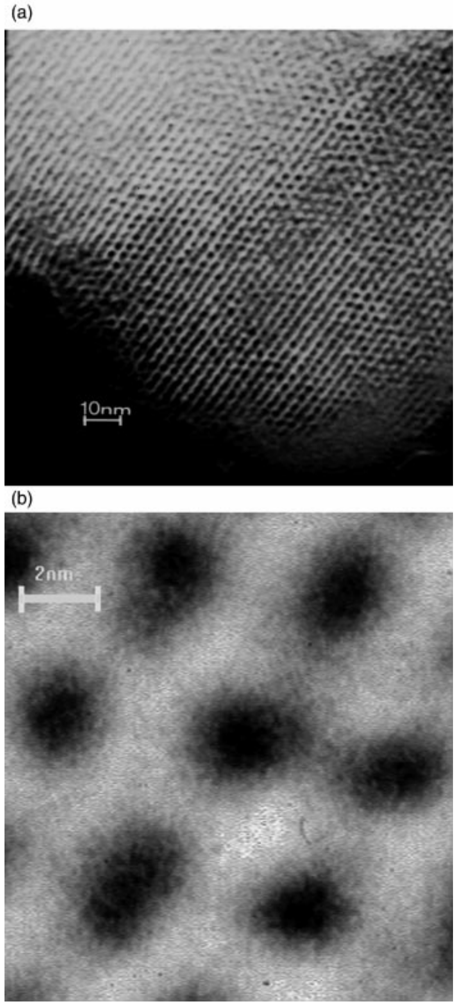

Fig. 3 (a) TEM micrograph for calcined MCM-Cu(1.2) and (b) an enlarged area of (a) showing the regular hexagonal arrangement of pores (dark); the light region is the silica network.

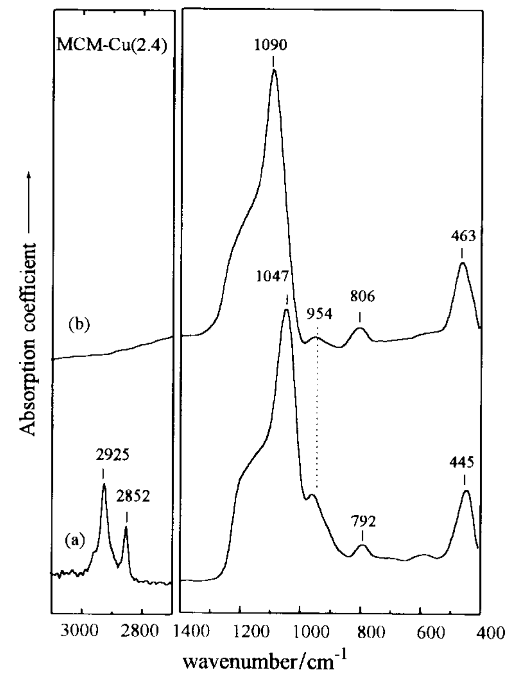

Fig. 4 IR absorption spectra for MCM-Cu(2.4): (a) as synthesized and (b) after calcination at 600 °C.

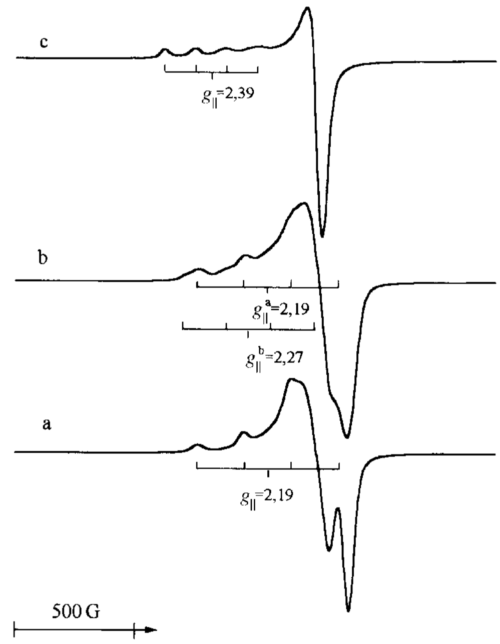

Fig. 5 EPR spectra of (a) frozen DIAMO–Cu solution, (b) as synthesized MCM-Cu(2.4) and (c) MCM-Cu(2.4) after calcination at 600 °C. The spectra were recorded at a temperature of 10 K.

template ions with a concomitant decrease in the number of Si–O$^-$ and Si–OH units. The removal of surfactant template is evident from the high wavenumber part of the spectrum where the absorption bands at 2925 and 2852 cm^{-1} from the asymmetric and symmetric vibrations of CH_2 units as well as the high frequency shoulder in the 2925 cm^{-1} band from the asymmetric vibration of the CH_3 group vanish upon calcination.

Location and coordination geometry of Cu^{2+} in MCM-41

In order to probe the location and environment of Cu^{2+} ions in the silica framework, low temperature EPR spectroscopy was employed. Fig. 5 shows the EPR spectra of (a) a precursor Cu-complex in a frozen methanol solution, (b) air-dried MCM-Cu(2.4) and (c) calcined MCM-Cu(2.4). The spectrum of the frozen Cu–DIAMO complex can be described by an axial spin Hamiltonian with parameters $g_{\|}=2.19$, $g_{\perp}=2.05$ and $A_{\|}=0.0180$ cm^{-1} which point to a square planar symmetry for Cu(II) ions coordinated to four nitrogens.[27–29] The spectrum of the as synthesized MCM-Cu(2.4) sample consists of two signals, probably arising from two different copper centers denoted "a" and "b". The more intense signal, assigned to center "a", can be described by an axial spin Hamiltonian with parameters $g_{\|}=2.19$, $A_{\|}=0.01810$ cm^{-1} and $g_{\perp}=2.05$. This set of parameters is similar to that observed for the Cu–DIAMO complex suggesting similar environments for Cu(II) ions in both samples. Thus we can assume that the greater part of Cu(II) ions is complexed by DIAMO in the as synthesized MCM-Cu(2.4) material. On the other hand, the signal of lower intensity, center "b", is described by $g_{\|}=2.27$ and $A_{\|}=0.0158$ cm^{-1}. In this case the parameter $g_{\perp}$ could not be determined because of overlap with the more intense $g_{\perp}$ part of center "a".

The observed differences in the EPR parameters between centers "a" and "b" can be attributed to a varying number of nitrogen coordinated sites and to a change in the symmetry of the species. According to a large number of Cu(II) EPR studies a $g_{\|}$ value in the range 2.27–2.29 is characteristic for two nitrogen coordination, a value of 2.23 for three nitrogen and a value of 2.20 for four nitrogen coordination.[27–30] Furthermore, values of $g_{\|}=2.27$ and $A_{\|}=0.01580$ cm^{-1} have been reported for distorted octahedral (or tetragonal) configuration and $g_{\|}=2.19$ and $A_{\|}=0.01810$ cm^{-1} for square planar symmetry.[30] According to these assignments signal "b" can be ascribed to Cu(II) ions in distorted octahedral symmetry with two nitrogens and four oxygens as ligating atoms, the latter from framework or water molecules. These species probably originate from partial destruction of one chelating moiety of the complex $\{[(CH_3O)_3Si(CH_2)_3NHCH_2CH_2NH_2]_2\}Cu$ during formation of the crystalline solid.

The spectrum of the calcined MCM-Cu(2.4) sample is shown in Fig. 5(c). In contrast to the spectrum of the as synthesized product that of the calcined material indicates the presence of only one species that can be described by an axial spin Hamiltonian with $g_{\|}=2.39$, $g_{\perp}=2.07$, $A_{\|}=0.0120$ cm^{-1}. These EPR parameters differ only slightly from the $g_{\|}$ and $A_{\|}$ values for $[Cu(H_2O)_6]^{2+}$ found in hydrated ion exchanged Cu-MCM-41, ($g_{\|}=2.4$, $A_{\|}=0.0141$ cm^{-1})[12,28] or hydrated clay minerals ($g_{\|}=2.38$, $A_{\|}=0.0145$ cm^{-1}).[31,32] Accordingly, we propose a similar octahedral geometry with a tetragonal elongation resulting from the coordination of Cu(II) to silica oxygens in MCM-Cu(2.4). It should be noted that the different $g_{\|}$ and $A_{\|}$ values for the as synthesized and calcined Cu-MCM materials may correspond to the same coordination geometry, since complete substitution of nitrogen ligands by framework oxygens would decrease $A_{\|}$ and increase $g_{\|}$.

Fig. 6 shows the EPR spectra of MCM-Cu(2.4) and MCM-Cu(4.7), in comparison with the spectrum of a reference MCM-41 sample (see Experimental section) containing 4.7 wt% Cu(II). The MCM-Cu(4.7) sample has nearly twice an intense EPR signal in comparison with the MCM-Cu(2.4) sample and almost the same intensity as that of the reference sample. Since all spectra were measured under the same conditions, the EPR intensities of the spectra should be directly proportional to the concentration of Cu(II) ions in these materials. The small discrepancies observed for the signal intensities between MCM-Cu(4.7) and the reference sample might be due to slight experimental variations in the EPR measurements.

Another important question concerns the accessibility of Cu(II) sites by other molecules penetrating into the mesoporous structure. In order to examine this, the calcined MCM-Cu(2.4) sample was exposed to pyridine vapour for a few hours and then its EPR spectrum was recorded. The spectra of the calcined MCM-Cu(2.4) sample before (a) and after pyridine exposure (b) are illustrated in Fig. 7. The observed axial signals

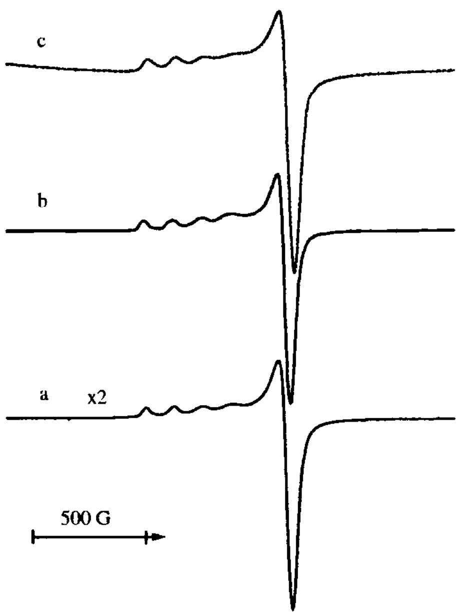

Fig. 6 EPR spectra for samples calcined at 600 °C: (a) MCM-Cu(2.4) and (b) MCM-Cu(4.7). (c) MCM-41 reference sample containing *ca.* 4.7 wt% copper. All spectra were recorded under the same conditions.

with $g_{\parallel}=2.39$, $g_{\perp}=2.07$, $A_{\parallel}=0.0120\ \mathrm{cm^{-1}}$ for the calcined MCM-Cu(2.4) changed to $g_{\parallel}=2.27$, $A_{\parallel}=0.0160\ \mathrm{cm^{-1}}$, $g_{\perp}=2.05$ after pyridine adsorption. The different parameters probably arise from the substitution of ligating oxygens by the nitrogen atoms of pyridine molecules. Based on these EPR parameters we suggest that the number of nitrogens coordinated to each copper(II) ion is probably one or at most two.[33] The symmetry of the species probably remains distorted octahedral or changed to trigonal-distorted planar symmetry with nitrogen from pyridine molecules and oxygens from the framework acting as ligands. In an EPR study of ion-exchanged Cu(II) ions into aluminium containing MCM-41,[27] the same experiment (adsorption of pyridine) did not alter the EPR signal even for long exposure times (30 days). The explanation for this different behaviour is that the Cu(II) ion sites are buried within the mesoporous walls and thus polar adsorbate molecules, such as pyridine, cannot gain access to them. On the other hand, the accessibility of Cu^{2+} centers in the present MCM-Cu(2.4) solid to pyridine, indicates that most of the copper(II) ions are located in the interior surfaces of the mesopores with a small portion of copper ions present inside the silicate walls.

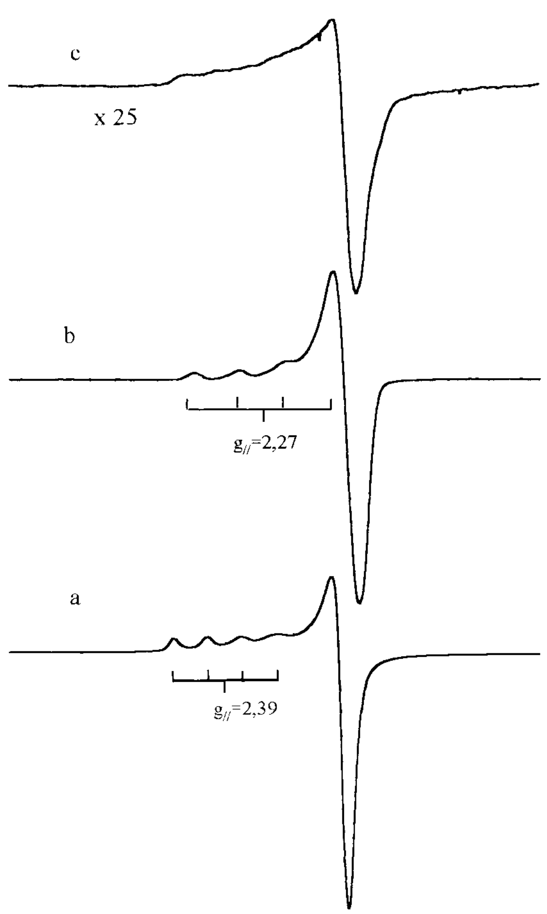

Fig. 7 EPR spectra of MCM-Cu(2.4) samples calcined at 600 °C: (a) initial spectrum, (b) after exposure to pyridine vapour for a few hours and (c) after treatment with NaI solution. The spectra were recorded at a temperature of 10 K.

The EPR spectrum of calcined MCM-Cu(2.4) was also measured after a reduction treatment with a solution of a NaI for a few hours. The spectrum of the reduced sample shows a 25 times lower intensity signal and a weaker hyperfine structure in comparison to that of untreated sample [Fig. 7(a)]. The intensity decrease can be attributed to the reduction of Cu(II) to Cu(I) which is EPR silent. Spectrum (c) also indicates that some of the Cu(II) species are unaffected by the reduction process probably because these ions are trapped into the mesoporous walls during the synthesis and are thus inaccessible to reductive reagents.

Electroactivity of copper containing MCM-41

Cyclic voltammetry (CV) of the as synthesized and calcined MCM-41 samples did not exhibit any electroactivity in acetonitrile in the potential range −1.5 to 0.7 V as a consequence of the absence of any redox centers (data not shown). Similarly, an as synthesized MCM-Cu(2.4) sample was electrochemically silent. This is expected because of the presence of surfactant molecules acting as templates in the synthesis of mesoporous materials. Electron transfer can occur only if the electroactive species are in contact with graphite particles in the composite electrode. Surfactant molecules, which are adsorbed on the external surfaces as well as those filling cylindrical pores, will strongly obstruct electron transfer between redox centers and the graphite particles.

By contrast, a calcined MCM-Cu(2.4) sample exhibits a marked electroactivity as shown in Fig. 8(a). This electroactivity can be ascribed to the presence of copper centers since calcined MCM-41 is electroinactive. The first cycle in Fig. 8(a) clearly shows one reduction peak P_c^1 at −447 mV associated with the anodic peak P_a^1 at −37 mV. A second redox system (peaks P_c^2 and P_a^2) of very weak intensity can be seen at more negative potentials. When the electrode potential is cycled to more negative potentials (−1.5 V), the reverse sweep is accompanied by a considerable enhancement of the anodic peak current intensity P_a^2 [Fig. 8(a), dotted line]. The peaks P_c^1 and P_c^2 are attributed to electrochemical reduction of Cu^{2+} and Cu^{+} ions and peaks P_a^1, P_a^2 to the electrochemical oxidation of reduced Cu^{+} and Cu^{2+}.[34]

Repetitive potential cycles between −370 mV and −1160 mV gives rise to a marked enhancement of the cathodic peak current P_c^2 [Fig. 8(b)]. This peak becomes stable regardless of the initial or final potential of the sweep. After cycling for 15 min a stable response is obtained from each of the redox systems 1 ($E_{pc}^1=-458$ mV, $E_{pa}^1=30$ mV) and 2 ($E_{pc}^2=-930$ mV, $E_{pa}^2=-420$ mV), Fig. 8(b). The peak intensities did not change with either immersion time or number of redox cycles. This suggests that the metal centers are strongly bound to the inorganic matrix. This set of electrochemical experiments unambiguously demonstrate the existence of redox active copper centers in calcined MCM-Cu(2.4). The electroactivity observed probably reflects the redox activity of copper

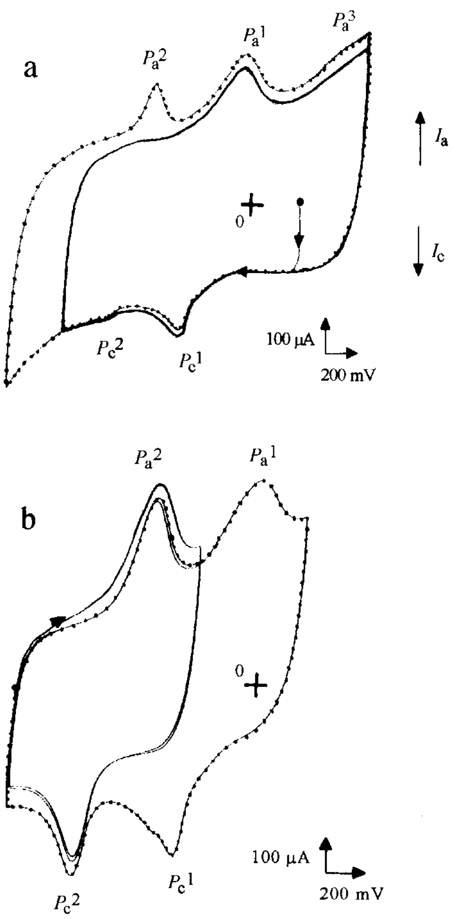

Fig. 8 Cyclic voltammograms of (a) a composite electrode containing calcined Cu–MCM-41 in CH_3CN (0.1 M TBAP) and (b) the same electrode after 15 min of continuous cycling between −3.70 and −1160 mV (b). The solid line corresponds to the first cycle and the dotted line to a second cycle after 15 min. Conditions: potential scan rate = 10 mV s^{-1}. Potentials are given *vs.* an Ag|Ag^+ 10 mM reference electrode.

centers located at or near the pore openings of the MCM-Cu(2.4) sample, since electron transfer can occur only if the electroactive species are in contact with the graphite particles of the composite electrode. This confirms further the observation by EPR that most of the copper centers are not located within the walls forming the mesopores, but are distributed on the surfaces of the mesoporous structure. The small portion of copper ions which are inside the walls are not detectable by electrochemical experiments.

Finally the amount of Cu ions on outer surfaces is small since the internal surface area of MCM-Cu(2.4) is calculated to be 1200 times greater than the outer surface. Furthermore, the experimental data for MCM-Cu(2.4) show that the surface area before surfactant extraction (where the total surface equals that of the outer surface area) is only 24 $m^2 g^{-1}$ whereas, the total surface area, after surfactant removal, is 988 $m^2 g^{-1}$. Since in the present work sol–gel synthesis was used to secure excellent homogeneous dispersion of various species in a silicate matrix, it is very likely that a large majority of the Cu complexes are dispersed in the interior pore surfaces.

Conclusions

Copper containing MCM-41 materials have been prepared by a route based on a sol–gel approach at room temperature. Remarkably, the amount of copper ion incorporated within the mesoporous silicate framework was significantly higher (4.7 wt%) in comparison to that obtainable by other known procedures (maximum 0.5 wt% Cu). It was found that a copper loading above *ca.* 2.5 wt% led to a progressive destruction of the long-range hexagonal order of the MCM-41 material. EPR experiments revealed a distorted octahedral geometry for copper ions, while polar molecules, such as pyridine, have easy access to these sites. Cyclic voltammetry of the calcined copper containing MCM-41 revealed a marked electroactivity for Cu^{2+} modified MCM-41 and demonstrated strong binding of the Cu^{2+} centers to the inorganic matrix as well as high stability.

Acknowledgements

The authors thank Dr A. Travlos for the TEM measurements.

References

1 J. S. Beck, J. C. Vartuli, W. J. Roth, M. E. Leonowicz, C. T. Kresge, C. T. Schmitt, C. T.-W. Chu, D. H. Olson, E. W. Sheppard, S. B. McCullen, J. B. Higgins and J. L. Schlenker, *J. Am. Chem. Soc.*, 1992, **114**, 10834.
2 J. S. Beck, J. C. Vartuli, G. J. Kennedy, C. T. Kresge, W. J. Roth and S. E. Schramm, *Chem. Mater.*, 1994, **6**, 1816.
3 Q. Huo, D. I. Margolese, U. Ciesla, P. Feng, T. E. Gier, P. Sieger, R. Leon, P. M. Petroff, F. Schuth and G. D. Stucky, *Nature*, 1994, **368**, 317.
4 A. Corma, M. T. Navarro and J. Perez-Parientes, *J. Chem. Soc., Chem. Commun.*, 1994, 1059.
5 Z. Luan, C-F. Cheng, W. Zhou and J. Klinowski, *J. Phys. Chem.*, 1995, **99**, 1018.
6 M. E. Davis, C.-Y. Chen, S. L. Burkett and R. F. Lobo, *Mater. Res. Soc. Symp. Proc.*, 1994, **346**, 831.
7 A. Tuel and S. Gontier, *Chem. Mater.*, 1996, **8**, 114.
8 T. M. Abdel-Fattah and T. J. Pinnavaia, *Chem. Commun.*, 1996, 665.
9 T. P. Tanev, M. Chibwe and T. J. Pinnavaia, *Nature*, 1994, **368**, 321.
10 N. Ulagappan and C. N. R. Rao, *Chem. Commun.*, 1996, 1047.
11 S. Ayyappan and C. N. R. Rao, *Chem. Commun.*, 1997, 577.
12 A. Pöppl, M. Newhouse and L. Kevan, *J. Phys. Chem.*, 1995, **99**, 100019.
13 M. Hartmmann, A. Pöppl and L. Kevan, *J. Phys. Chem.*, 1996, **100**, 9906.
14 A. Kucherov and A. A. Slinkin, *J. Mol. Catal.*, 1994, **90**, 323.
15 T. Maschmeyer, F. Rey, G. Sankar and J. M. Thomas, *Nature*, 1995, **378**, 159.
16 D. Zhao and D. Goldfarb, *J. Chem. Soc., Chem. Commun.*, 1995, 875.
17 Z. Y. Yuan, S. Q. Liu, T. H. Chen, J. Z. Wang and H. X. Li, *J. Chem. Soc., Chem. Commun.*, 1995, 973.
18 M. A. Karakassides, K. G. Fournaris and D. Petridis, *Adv. Mater.*, 1998, **10**, 483.
19 S. L. Burkett, S. D. Sims and S. Mann, *Chem. Commun.*, 1996, 1367.
20 M. T. Anderson, J. E. Martin, J. Odinek and P. Newcomer, *Access in Nanoporous Materials*, Plenum Press, New York and London, 1995, pp. 29–37.
21 C. Rierce, *J. Phys. Chem.*, 1953, **57**, 149.
22 P. T. Tanev and T. J. Pinnavaia, *Chem. Mater.*, 1996, **8**, 2068.
23 C. T. Kirk, *Phys. Rev. B*, 1988, **38**, 1255.
24 P. G. Pai, S. S. Chao, Y. Takagi and G. Lucovsky, *J. Vac. Sci. Technol. A*, 1986, **4**, 689.
25 M. R. Almeida and C. G. Pantano, *J. Appl. Phys.*, 1990, **68**, 4225.
26 E. I. Kamitsos, A. P. Patsis and G. Kordas, *Phys. Rev. B*, 1993, **48**, 12499.
27 A. Pöppl, M. Hartmann and L. Kevan, *J. Phys. Chem.*, 1995, **99**, 17251.
28 M. Yonemitsu, Y. Tanaka and M. Iwamoto, *Chem. Mater.*, 1997, **9**, 2679.
29 J. F. Diaz, K. J. Jr. Balkus, F. Bedioui, V. Kurshev and L. Kevan, *Chem. Mater.*, 1997, **9**, 61.
30 R. Barbucci and M. J. M. Campbell, *Inorg. Chim. Acta*, 1976, **16**, 113.
31 J.-M. Comets, V. Luca and L. Kevan, *J. Phys. Chem.*, 1992, **96**, 2645.
32 M. Mc Bride, T. J. Pinnavaia and M. M. Mortland, *J. Phys. Chem.*, 1975, **79**, 1975.
33 H. Tominaga, Y. Ono and T. Keii, *J. Catal.*, 1975, **40**, 197.
34 J. Li and G. Calzaferri, *J. Electroanal. Chem.*, 1994, **377**, 163.

Paper a904545g